Journal of Solid State Chemistry 183 (2010) 584–589

Contents lists available at ScienceDirect

Journal of Solid State Chemistry

journal homepage: www.elsevier.com/locate/jssc

Preparation and up-conversion fluorescence of rare earth (Er^{3+} or Yb^{3+}/Er^{3+})-doped TiO_2 nanobelts

Tianhao Ji [a,*], Yang Liu [a], Hui Zhao [a], Haiyan Du [a], Jiayue Sun [a], Guanglu Ge [b]

[a] College of Chemical and Environmental Engineering, Beijing Technology and Business University, 11 Fucheng Road, Beijing 100048, China
[b] National Center for Nanoscience and Technology, Beijing 100190, China

ARTICLE INFO

Article history:
Received 2 October 2009
Received in revised form
2 January 2010
Accepted 5 January 2010
Available online 11 January 2010

Keywords:
TiO_2 nanobelts
Rare earth doping
Hydrothermal
Up-conversion

ABSTRACT

Anatase TiO_2 nanobelts doped with rare earth (*RE*) ions Yb^{3+}, Er^{3+} or Yb^{3+}/Er^{3+} have been prepared using layered titanate nanobelts (LTO NBs) with *RE* ions as the precursor obtained by ion-exchange between LTO NBs and *RE* ions under hydrothermal process. Various measurement results demonstrate that the *RE* ions have doped into the lattice of TiO_2, and the Er^{3+} or Yb^{3+}/Er^{3+} doped nanobelts show strong visible up-conversion (UC) fluorescence under 980 nm excitation. The UC emission intensity of LTO NBs embedded with Er^{3+} or Yb^{3+}/Er^{3+} is slightly higher than that of the corresponding TiO_2 nanobelts doped with *RE* ions, whereas higher *RE* doping content leads to the decrease of UC emission intensity due to the concentration-quenching effect.

1. Introduction

One-dimensional (1D) semiconductor nanowires or nanobelts have been intensively explored in various fields of optoelectronic devices in the past several years, such as nanolasers, microcavity lasers, sensors, photodetectors or solar cell [1–4]. In order to improve the optoelectronic properties of 1D nano-devices, the preparation of single crystalline structure is usually desired, and other aspects, such as large aspect ratio or metal ions doping, are also often considered. It has been demonstrated that the single crystalline structure of 1D semiconductor can indeed modify the optoelectronic properties of nano-devices due to the decrease of defect effect and electron–hole recombination. The doping of metal ions, especially rare-earth (*RE*) ions into the structure, can not only improve optoelectronic property, but also tune the emission position and intensity.

To the best of our knowledge, although various *RE*-doped semiconductor nano-materials have been widely investigated, few *RE*-doped single crystalline 1D semiconductor oxides were prepared except for the reports of the *RE*-doped ZnO nanowires, Eu-doped $MgBO_2(OH)$ or Y_2O_3 nanobelts [5–9]. In particular, there are no reports for *RE*-doped TiO_2 nanowires or nanobelts owing to the challenge of preparing oxide with *RE* ions and the uniformity of such doping ions in such structure. It is well known that TiO_2 is very important wide-band-gap semiconductor widely used in many fields. TiO_2 nanowires or nanobelts have also been demonstrated to exhibit promising photocatalysis because of lower electron–hole recombination rate than the nanospheric counterpart [10], thus they will have significant optoelectronic property and potential application in solar cell. To improve the photoelectrical energy conversion efficiency of solar cell, one often search for the integrated semiconductor material with strong visible-light absorption, high charge transport, low electron–hole recombination, low heat-loss and low cost. Based on the above considerations, TiO_2 nanobelts as host matrix are first chosen to prepare up-conversion nano-oxide with *RE* doping cations (*RE*=Er^{3+} or Yb^{3+}/Er^{3+}). *RE*-doped upconversion oxide nanoparticles, such as Er-doped ZrO_2, TiO_2 or $BaTiO_3$ nanoparticles, have been prepared previously [11–13], whereas in this study, *RE*-doped TiO_2 nanobelts with strong upconversion fluorescence will be reported in detail.

TiO_2 nanobelts with Yb^{3+}, Er^{3+} or Yb^{3+}/Er^{3+} cations were synthesized using two-step preparation process of ion-exchange and hydrothermal treatment. Various measurement techniques were performed to demonstrate the doping of the rare earth cations into the lattice of TiO_2 nanobelts. Upconversion fluorescence measurements of layered titanate nanobelts and TiO_2 nanobelts with Er^{3+} or Yb^{3+}/Er^{3+} were recorded at room temperature and fluorescence emission mechanism was discussed as well.

2. Experimental

2.1. Chemicals

All the chemicals were of analytical grade and used as received without further purification. Deionized water was used through-

* Corresponding author.
E-mail address: jitianhao@th.btbu.edu.cn (T. Ji).

0022-4596/$ - see front matter © 2010 Elsevier Inc. All rights reserved.
doi:10.1016/j.jssc.2010.01.004

out the experiment. $Er(NO_3)_3 \cdot 6H_2O$, $Yb(NO_3)_3 \cdot 6H_2O$ (purity > 99.9%) were purchased from the Shanghai Chemical Reagent Company. NaOH and HCl were supplied by the Beijing Chemical Reagent Company.

2.2. Preparation of RE-TiO_2 nanobelts

First of all, layered titanate nanobelts (LTO NBs) were obtained under hydrothermal condition in Teflon-lined autoclave with a mixture of TiO_2 nanoparticles and 10 M NaOH aqueous solution as reported previously [14]. It should be stressed that the as prepared LTO NBs need to be immersed in 2 M HCl to avoid the formation of the by-product of rare earth hydrolysate before ion-exchange process is carried out. The prepared LTO NBs were mixed with different concentration of *RE* cations (*RE*=Yb^{3+}, Er^{3+} or Yb^{3+}/Er^{3+}) aqueous solution at room temperature in 50-mL autoclave, and then ion-exchange reaction occurred between *RE* cations in solution and H^+ in LTO NBs at 120 °C for 20 h to form LTO NBs with *RE* cations (*RE*-LTO NBs). The *RE*-LTO NBs were further treated in purely deionized water at 160 °C for several hours to prepare *RE*-doped TiO_2 nanobelts. For comparison, the TiO_2 nanobelts without any *RE* ions (TiO_2 NBs) were also synthesized under the same preparation process. The detail preparation condition and actual compositions of *RE*-doped TiO_2 NBs are shown in Table 1.

2.3. Characterization

The products with or without rare earth cation doping were characterized by powder X-ray diffraction (XRD) with a Shimadzu XRD-6000 diffractometer equipped with monochromatic high-intensity Cu*K*α radiation (λ=0.154056 nm). Scanning electron microscope (SEM) with energy-dispersive X-ray (EDX) analysis was taken on JEOL-JSM 6490. Transmission electron microscopy (TEM) and high-resolution transmission electron microscopy (HRTEM) images were measured on JEOL JEM-2010 and JEOL-2010 with EDX at an acceleration voltage of 200 kV, respectively. Elemental compositions (*RE*:Ti) were analyzed by inductively coupled plasma-mass spectrometry (ICP-MS) on PE-ELAN6000. X-ray photoelectron spectroscopy (XPS) measurements were performed on ESCALAB-250. Up-conversion luminescence was analyzed by Hitachi F4500 fluorescence spectrophotometer combined with 980 nm semiconductor-pumped laser source. Fourier transform infrared (FTIR) spectra were measured on Nicolet Avata 370.

Table 1
RE-to-Ti molar ratios and actual compositions of *RE*-doped TiO_2 NBs.

Materials	*T* (°C)	*t* (h)	n_{Yb}: n_{Ti}[a]	n_{Er}: n_{Ti}[a]	Actual composition
TiO_2 NBs	160	20	–	–	TiO_2
RE-TiO_2-01	160	20	0.1251	0.0401	$Ti_{0.858}Yb_{0.108}Er_{0.034}O_2$
RE-TiO_2-02	160	20	0.0609	0.0131	$Ti_{0.931}Yb_{0.057}Er_{0.012}O_2$
Yb-TiO_2-01	160	20	0.0768	–	$Ti_{0.929}Yb_{0.071}O_2$
Er-TiO_2-01	160	20	–	0.0556	$Ti_{0.947}Er_{0.053}O_2$
Yb-TiO_2-02	160	20	0.1418	–	$Ti_{0.876}Yb_{0.124}O_2$
Er-TiO_2-02	160	20	–	0.1239	$Ti_{0.890}Er_{0.110}O_2$

[a] ICP-MS analysis.

3. Result and discussion

The XRD patterns of the products *RE*-TiO_2-01, *RE*-TiO_2-02, Er-TiO_2-01, Yb-TiO_2-01 and TiO_2 NBs are shown in Fig. 1. The preparation condition and rare earth content of these samples are presented in Table 1. All of the peaks in the XRD patterns match very well with the standard tetragonal anatase TiO_2 crystal structure data (JCPDS No. 21-1272). No other patterns of impurities can be observed, whereas the ICP-MS measurement results show the existence of the Yb/Er, Er or Yb rare earth elements. The doping of Er^{3+} or/and Yb^{3+} cations into the lattice structure will results from the shift of diffraction peaks since the ion radii of Er^{3+} and Yb^{3+} (0.088 and 0.099 nm, respectively) are different from the radius of Ti^{4+} (0.061 nm) cations. From the (101) peak, we have indeed observed such shift to low diffraction angle as shown in Fig. 1b after *RE* cations were added into the TiO_2 NBs, indicating that they have been doped into the lattice structure of the TiO_2 NBs, but a slight shift also reveals the effect of other case such as defects of oxygen vacancies on the structure [15–17].

Fig. 2 presents the SEM micrographs and EDX mappings of the Er-TiO_2-02 and Yb-TiO_2-02 samples. The LTO NBs embedded with Er^{3+} or Yb^{3+} cations, existed between the two Ti–O layers of the LTO NBs, were first prepared using ion-exchangeable process prior to the formation of TiO_2 NBs doped with Er^{3+} or Yb^{3+}. The LTO NBs with Er^{3+} or Yb^{3+} observed from Fig. 2(a) or (b) shows smooth surface and nanobelt-shape. It should be stressed that the layered sodium titanate prepared from 10 M NaOH solution should be first immersed into 2 M HCl aqueous solution for a long time so that the Na^+ between Ti–O layers can be substituted for H^+, and subsequently, the LTO NBs with *RE* cations can be obtained by ion-exchange between the LTO NBs with H^+ and *RE* cations. After the LTO nanobelts with *RE* cations are treated and

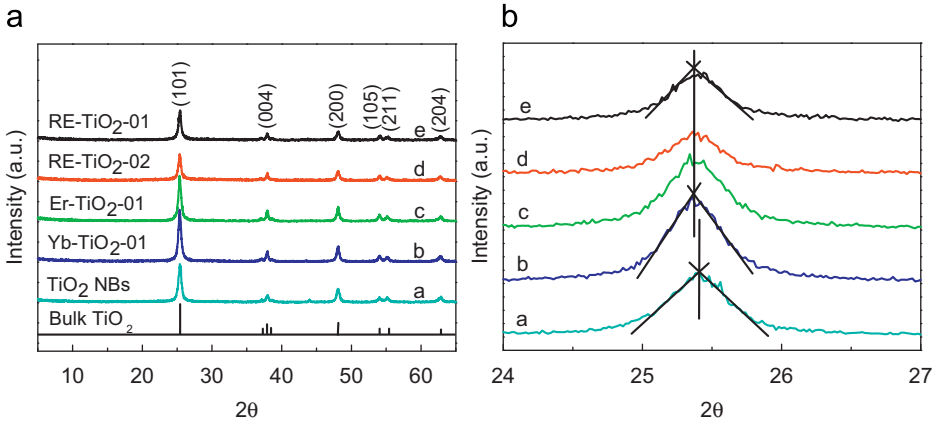

Fig. 1. Powder XRD patterns of the products TiO_2 NBs (a), Yb-TiO_2-01(b), Er-TiO_2-01 (c), *RE*-TiO_2-02 (d) and *RE*-TiO_2-01 (e).

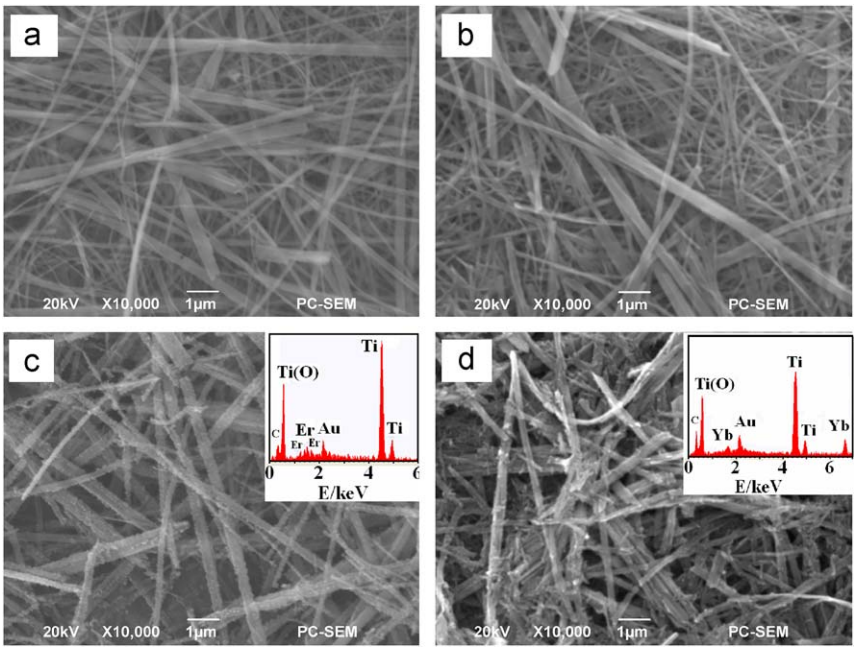

Fig. 2. SEM images of the Er-LTO-02 (a), Yb-LTO-02 (b), Er-TiO_2-02 (c) and Yb-TiO_2-02 (d). Insets are the corresponding EDX mappings.

transferred into Er-doped TiO_2 or Yb-doped TiO_2 at 160 °C for 20 h in autoclave, the doped TiO_2 still remains the nanobelt-shape, whereas the surface becomes much rougher, resulted from the phase transformation from layered titanate to anatase phase TiO_2. The EDX elemental mappings shown in the inset of the SEM images identify the distribution and content of elements Er or Yb, Ti and O. The mappings demonstrate the existence of Er or Yb element for the four samples. The calculated atomic ratios for the Er-TiO_2-02 and Yb-TiO_2-02 are 0.0136 and 0.0154, respectively, in good agreement with the ICP-MS analysis results in Table 1.

The phase transformation process and mechanism of LTO NBs into anatase TiO_2 NBs under hydrothermal condition have been reported previously by Mao and Wong [18]. They made conclusion that as-formed anatase TiO_2 NBs attaching to layered titanate nanowires aggregated and further fused to form anatase TiO_2 NBs, thereby the surface of the formed TiO_2 NBs became much rougher. However, based on a large number of experimental results published by the literatures [15,19], it has been revealed that the phase transformation from LTO NBs to anatase TiO_2 NBs was resulted from the crystalline lattice shrinkage. As the distance between two nearest-neighbored layers in LTO NBs is about 0.8 nm, the layered structure of LTO NBs disappears under hydrothermal treatment owing to the thermal vibration of the Ti–O layers and further dehydration reaction between the two nearest-neighbored layers, and then the LTO NBs become the most stable anatase TiO_2 NBs.

The SEM, TEM and HRTEM micrographs of the *RE*-TiO_2-01 and *RE*-TiO_2-02 are shown in Fig. 3. Similar to the morphology of the LTO NBs with Er^{3+} or Yb^{3+} in the above Figs. 2(a) and (b), the LTO NBs co-embedded with Yb^{3+}/Er^{3+} are still nanobelt-shape and the surface is also very smooth (Figs. 3(a) and (b)). After they are transferred into anatase phase TiO_2, their nanobelt-shape is kept very well, thus the codoping of the Yb^{3+}/Er^{3+} cations has hardly changed such shape, but the surface becomes a little rough. The EDX elemental mappings shown in the inset reveal the existence of Yb, Er and Ti elements.

The rough surface of the *RE*-TiO_2-01 can be observed clearly from the TEM image as shown in Fig. 3(e). The HRTEM image in Fig. 3(f) shows the lattice structure of a part of one nanobelt in Fig. 3(e). It depicts well-defined lattice fringes (101) with 0.352 nm interplanar spacing, which is perpendicular to the [101] orientation of the TiO_2 nanobelt, in good agreement with the strongest (101) peak in the above XRD measurement. Such [101] orientation is not the nanobelt orientation, also demonstrated in our previous report [19]. Owing to the existence of a large number of the Yb^{3+}/Er^{3+} cations in the lattice structure of the TiO_2 nanobelt, the notable dislocation defect as shown in the arrow has been observed. As the *RE*-TiO_2-01 with 10.8 at% Yb and 3.4 at% Er contains so many *RE* cations and the *RE* radii are obviously different from that of Ti^{4+}, there must have such dislocations after the formation of anatase phase *RE*-doped TiO_2 from *RE*-LTO NBs.

In order to investigate the uniformity of co-dopant Yb^{3+}/Er^{3+} in TiO_2 lattice, the EDX elemental mapping images of the ten positions on the single Yb^{3+}/Er^{3+}-codoped TiO_2 nanobelt for the *RE*-TiO_2-01 were measured as shown in Fig. 4. The Cu peaks are caused by used Cu-grid, and the Er, Yb, Ti and O element peaks are also clearly observed. The atomic ratios of the Er, Yb and Ti on the corresponding ten positions of such nanobelt have been given on the right-hand side of the figure. All of them are very close to the ICP-MS measurement results, and also they are very similar to each other. Therefore, the measurement results show that, to some extent, the distribution of Yb^{3+}/Er^{3+} cations in the nanobelt is relatively uniform.

XPS measurements of the *RE*-LTO-01 and *RE*-TiO_2-01 were performed to obtain the information of the Er and Yb oxidation state in the LTO or TiO_2 NBs. The survey and high-resolution XPS spectra are shown in Fig. 5. The two survey spectra have the similar curves, and further reveal that there has not any change for the chemical valence of compositional elements after the formation of TiO_2 NBs with Yb/Er (Fig. 5(a)). Such conclusion can also be supported by the high-resolution spectra of Er $4d_{5/2}$ and Yb $4d_{5/2}$ as well as Ti 2*p* in Figs. 5(b) and (c). The binding energies of the Er $4d_{5/2}$ and Yb $4d_{5/2}$ appeared at ca. 168.0 and 184.0 eV correspond to the energies of the Er^{3+} and Yb^{3+} photoelectrons [20]; the Ti 2*p* spectra shown at 459.0 and 465.0 eV assign to the binding energies of Ti $2p_{3/2}$ and Ti $2p_{1/2}$ for Ti^{4+} ions, respectively [21]. However, there still exists slight distinct between the shape

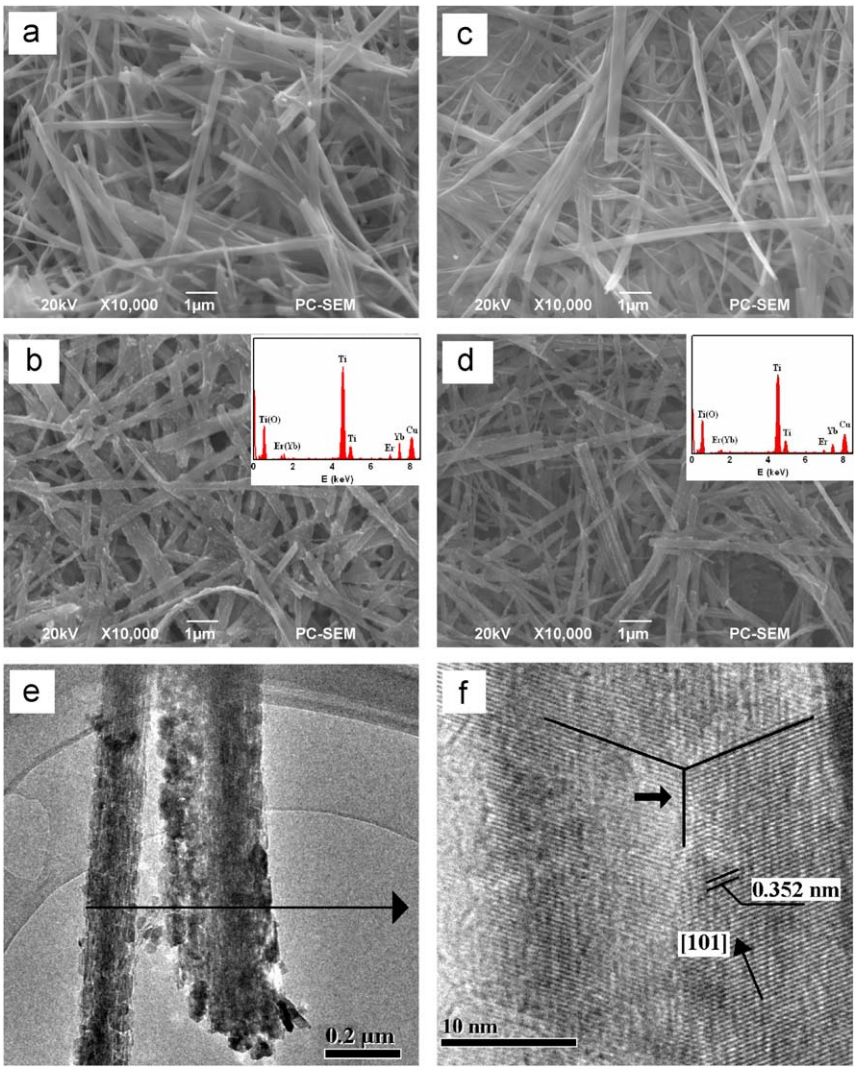

Fig. 3. SEM and TEM images of the *RE*-TiO_2-01 and *RE*-TiO_2-02: (a) SEM image of the *RE*-LTO-01; (b) SEM image of *RE*-TiO_2-01 (inset is the EDX mapping); (c) SEM image of *RE*-LTO-02; (d) SEM image of *RE*-TiO_2-02 (inset is the EDX mapping); (e) TEM image of *RE*-TiO_2-01; (f) HRTEM image of *RE*-TiO_2-01. The *RE*-LTO-01 and *RE*-LTO-02 are the layered titanate with Yb and Er codoping cations before the *RE*-TiO_2-01 and *RE*-TiO_2-02 are treated, respectively.

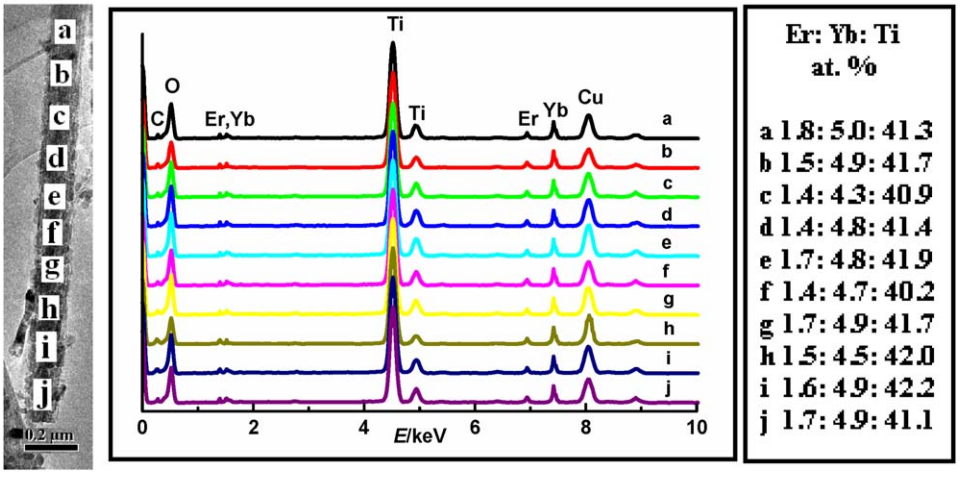

Fig. 4. EDX mapping images of the ten positions on the single Yb/Er-doped TiO_2 nanobelt of the *RE*-TiO_2-01.

of Er 4*d*, Yb 4*d* or Ti 2*p* peaks for the *RE*-TiO_2-01 and *RE*-LTO-01, interpreted that the Er^{3+}, Yb^{3+} and Ti^{4+} cations have different chemical environment before and after the formation of TiO_2 NBs.

Besides the above measurement results have proved the existence and doping of *RE* cations in the structure of the TiO_2 nanobelts, the up-conversion (UC) emission property can also

directly support the doping behavior. Fig. 6 is the UC fluorescence emissions of the Er-doped TiO_2 nanobelts (Er-TiO_2-01 and Er-TiO_2-02) and Yb/Er-codoped TiO_2 nanobelts (*RE*-TiO_2-01 and *RE*-TiO_2-02) recorded under 980 nm of excitation wavelength at room temperature. For the comparison, the UC fluorescence emissions of the LTO NBs with Er^{3+} or Yb^{3+}/Er^{3+} for the Er-LTO-01 or *RE*-LTO-01 as the precursor of the Er-TiO_2-01 or *RE*-TiO_2-01 are also set into the figure. The UC emissions are composed of two regions of 520–570 and 630–680 nm: the former is assigned to the strong green emission for the $(^2H_{11/2}, {}^4S_{3/2}) \rightarrow {}^4I_{15/2}$ transition and the latter is ascribed to the weak red emission for the $^4F_{9/2} \rightarrow {}^4I_{15/2}$ transition of the Er^{3+} dopants in the D_{4h} site of anatase TiO_2 nanobelts. In Fig. 6(a), the intensities of the three UC emission peaks for the Er-LTO-01, Er-TiO_2-01 and Er-TiO_2-02 have obviously different, in which that of the Er-LTO-01 is the strongest and that of the Er-TiO_2-02 is the weakest; In Fig. 6(b), the intensity of the *RE*-LTO-01 for the green emission is also slightly higher than that of the *RE*-TiO_2-01 and much higher than that of the *RE*-TiO_2-02, but the weak red emission resulted from the relatively low Er concentration demonstrated by the literature [22], can only be clearly observed under magnification as shown in the inset. Furthermore, the results indicate that the UC emission of LTO NBs embedded with Er^{3+} or Yb^{3+}/Er^{3+} shows significantly optical behaviors, whereas for the TiO_2 nanobelts doped with Er^{3+} or Yb^{3+}/Er^{3+} cations, higher dopant content is not of benefit for the UC emission intensity.

At present, it is well known that hexagonal $NaYF_4$ is the most efficient NIR-to-visible UC host due to the lowest phonon

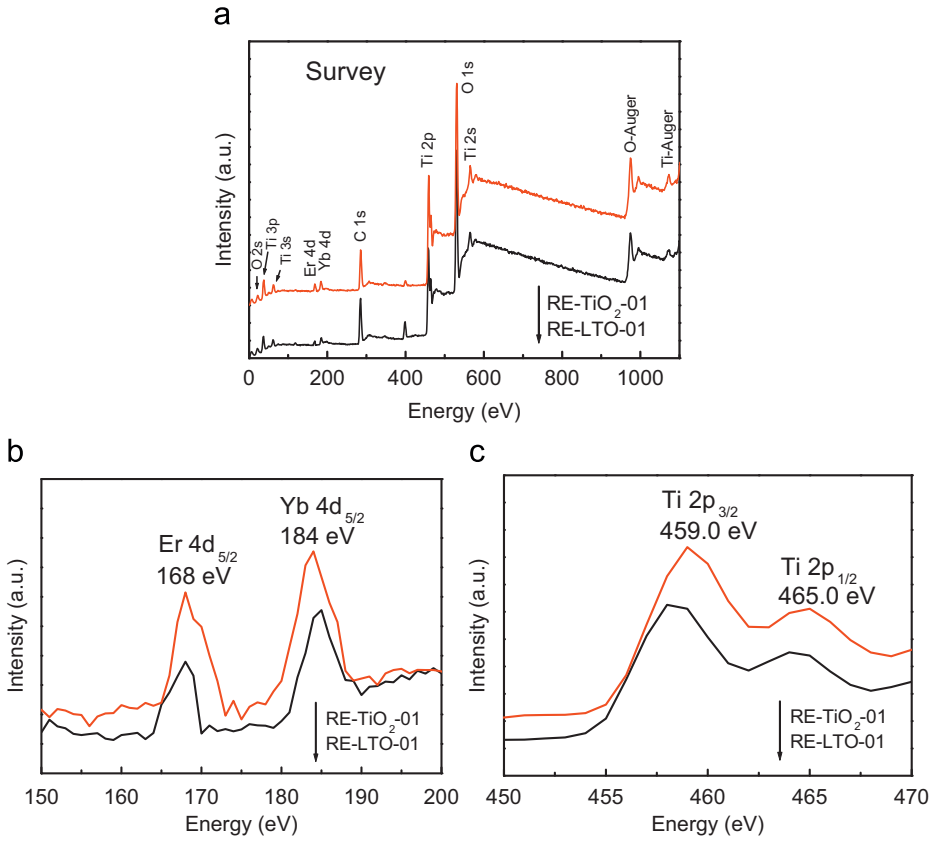

Fig. 5. Survey scan (a), Er 4*d* or Yb 4*d* (b) and Ti 2*p* (c) XPS spectra of the *RE*-LTO-01 and *RE*-TiO_2-01 recorded at room temperature.

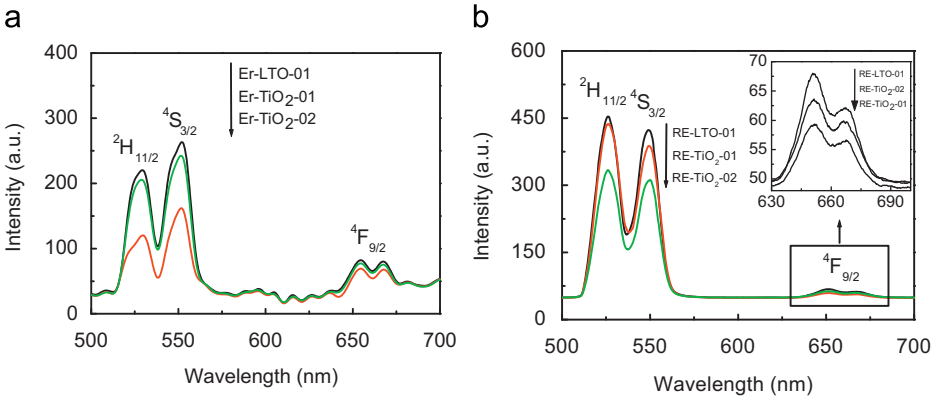

Fig. 6. UC fluorescence emission spectra of the *RE*-doped TiO_2 nanobelts (λ_{ex}=980 nm): (a) the Er-TiO_2-01 and Er-TiO_2-02; (b) the *RE*-TiO_2-01 and *RE*-TiO_2-02 (inset is the magnified spectrum around wavelength 660 nm). For comparison, the UC emission spectra of the Er-LTO-01 and *RE*-LTO-01 as the precursors of the Er-TiO_2-01 and *RE*-TiO_2-01 are also listed in the figure.

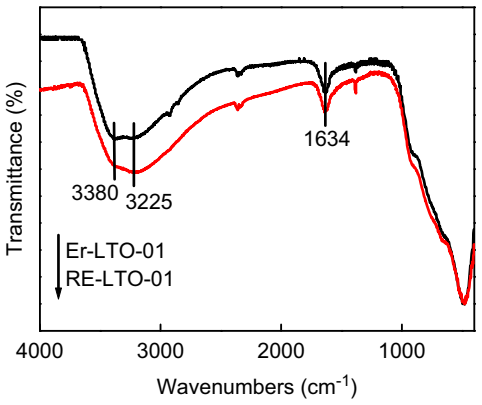

Fig. 7. FTIR spectra of the two samples Er-NTO-01 and *RE*-NTO-01.

frequency, but TiO_2 nanobelts as host matrix will enlarge the application in the optoelectronic field. As TiO_2 matrix has higher phonon frequency ($\sim$641 cm^{-1}), it increases the probability of multiphonon nonradiative process according to the Miyakawa–Dexter equation $W_p = W_o \exp[-\alpha\Delta E/(\hbar\omega)]$, and to some extent, it decreases the intensity of UC fluorescence emission [23]. The above UC emission measurement indeed reveals the relatively lower intensity by compared with that of the Er^{3+}- or Yb^{3+}/Er^{3+}-doped $NaYF_4$ reported previously [24].

The UC fluorescence mechanism of Er^{3+} or Yb^{3+}/Er^{3+} doping materials shown in energy level diagram contains excited-state absorption (ESA) of two photons of NIR light and energy-transfer up-conversion (ETU). The energy level diagram, describing the UC emission of oxide powders doped with Er^{3+} or Yb^{3+}/Er^{3+}, has been given in many literatures [25,26]. The wavelength position of UC emission is determined by different energy level of Er^{3+} ions, whereas the luminance value of UC emission intensity depends not only on the doping concentration of Er^{3+} cations, but also on the environment around Er^{3+} cations. The mean distance (R) between the dopant Er^{3+} or Yb^{3+}/Er^{3+} cations can be estimated by the equation $R = 0.62/(N)^{1/3}$ [13,27]. According to the calculation results, the R values of the Er-TiO_2-01 (5.3 mol% of Er^{3+}) and Er-TiO_2-02 (11.0 mol% of Er^{3+}) are 0.65 and 0.51; the R values of the *RE*-TiO_2-01 (14.2 mol% of Yb^{3+}/Er^{3+}) and *RE*-TiO_2-02 (6.9 mol% of Yb^{3+}/Er^{3+}) are 0.47 and 0.60, respectively. The higher concentration of Er^{3+} doping ions leads to the lower R value, thereby the distance between two Er^{3+} ions becomes smaller, and as a result for the Er-TiO_2-02, the concentration-quenching effect causes more predominant nonradiative decay process. The concentration-quenching effect reported in the literature [13,22] is the phenomenon of the emission decrease with the increase of rare earth activator such as Er^{3+} or Tm^{3+} due to nonradiative energy loss. However, the influence of such effect on the emission intensity of the *RE*-TiO_2-01 and *RE*-TiO_2-02 gets weaker because of the much lower Er concentration. In addition, the slightly higher behavior of the UC emission intensity of the corresponding *RE*-LTO NBs before the formation of the Er-TiO_2-01 and *RE*-TiO_2-01 can be interpreted by different chemical environment around Er^{3+} ions. Since the *RE* ions easily coordinate with water molecules, the Er^{3+} or Yb^{3+}/Er^{3+} embedded between the two nearest-neighbored layers also surround by water molecules, demonstrated by the FTIR measurement result as shown in Fig. 7 (the wavenumbers 3380, 3225 and 1634 cm^{-1} are assigned to those of symmetrical stretching vibration, asymmetrical stretching vibration and bending vibration of the coordinated H_2O in the Er-LTO-01 and *RE*-LTO-01, respectively), thus crystal field strength applied on the Er^{3+} cations becomes stronger and nonradiative quenching process is decreased, supported by Unal and co-workers' the measurement results that the water-coordinated Eu^{3+} cations in the interlayer of Ti–O layered oxide nanosheets show higher emission intensity than that of Eu^{3+} cations without surrounding water [28,29].

4. Conclusions

Er- or Yb-doped and Yb/Er-codoped TiO_2 nanobelts can be prepared using ion-exchange and hydrothermal treatment process. Such dopant rare earth cations have neither affected on nanobelt-shape nor changed the formation of anatase phase, whereas their doping causes many defects in the lattice structure of TiO_2 nanobelts. The distribution of the Yb/Er-codoping cations in TiO_2 lattice is relatively uniform. The UC fluorescence emissions of Er- or Yb/Er-codoped samples with different doping concentration can be obviously observed, showing that the emission intensity of layered titanate nanobelts embedded with Er^{3+} or Yb^{3+}/Er^{3+} cations shows slightly higher by compared with that of corresponding *RE*-doped anatase TiO_2 nanobelts, and also the higher *RE*-doping concentration leads to the decrease of UC emission intensity.

Acknowledgments

The work was supported by the "973" Basic Research Foundation of China (no. 2006CB932605), the National Natural Science Foundation of China (no. 20976002) and the Beijing Natural Science Foundation (no. 2091002).

References

[1] J.C. Johnson, H.J. Choi, K.R. Knutsen, R.D. Schaller, P.D. Yang, R.J. Saykally, Nat. Mater. 1 (2002) 106.
[2] Y.K. Liu, J.A. Zapien, C.Y. Geng, Y.Y. Shan, C.S. Lee, Y. Lifshitz, S.T. Lee, Appl. Phys. Lett. 85 (2004) 3241.
[3] L.H. Qian, K. Wang, Y. Li, H.T. Fang, Q.H. Lu, X.L. Ma, Mater. Chem. Phys. 100 (2006) 82.
[4] X. Wang, J. Song, Z.L. Wang, J. Mater. Chem. 17 (2007) 711.
[5] P. Mohanty, B. Kim, J. Park, Mater. Sci. Eng. B 138 (2007) 224.
[6] Y.S. Chen, T.Y. Tseng, J. Nanosci. Nanotechnol. 8 (2008) 4514.
[7] J. Wang, S.K. Hark, Q. Li, Microsc. Microanal. 12 (2006) 748.
[8] J.P. Liu, Y.Y. Li, X.T. Huang, Chem. Mater. 20 (2008) 250.
[9] Y. He, Y. Tian, Y.F. Zhu, Chem. Lett. 32 (2003) 862.
[10] J. Xie, H.Y. Zhang, X.H. Ou-yang, T.H. Ji, Z.Y. Xiao, J.Y. Sun, J. Inorg. Mater. 23 (2008) 262.
[11] R.K. Jia, W.S. Yang, Y.B. Bai, T.J. Li, Opt. Mater. 28 (2006) 246.
[12] Z. Zhou, T. Komori, T. Ayukawa, A. Koizumi, N. Matsunami, Y. Takeda, M. Morinaga, Opt. Mater. 28 (2006) 727.
[13] A. Patra, C.S. Friend, R. Kapoor, P.N. Prasad, Chem. Mater. 15 (2003) 3650.
[14] J. Xie, T.H. Ji, X.H. Ou-yang, Z.Y. Xiao, H.J. Shi, Solid State Commun. 147 (2008) 226.
[15] H.Y. Zhang, T.H. Ji, L.L. Li, X.Y. Qi, Y.F. Liu, J.W. Cai, H.Y. Du, J.Y. Sun, Acta Phys. Chim. Sin. 24 (2008) 607.
[16] Z.J. Hu, Y.S. Wang, F. Bao, W.Q. Luo, J. Non-Cryst. Solids 351 (2005) 722.
[17] D.Q. Chen, Y.S. Wang, Y.L. Yu, E. Ma, Mater. Chem. Phys. 101 (2007) 464.
[18] Y.B. Mao, S.S. Wong, J. Am. Chem. Soc. 128 (2006) 8217.
[19] H.Y. Zhang, T.H. Ji, Y.F. Liu, J.W. Cai, J. Phys. Chem. C 112 (2008) 8604.
[20] X.L. Ren, L.P. Li, Q. Wei, Chem. J. Chin. Univ. 16 (1995) 454.
[21] K.V.R. Chary, G.V. Sagar, D. Naresh, K.K. Seela, B. Sridhar, J. Phys. Chem. B 109 (2005) 9437.
[22] J.L. Zhuang, L.F. Liang, H.H.Y. Sung, X.F. Yang, M.M. Wu, L.D. Williams, S.H. Feng, Q. Su, Inorg. Chem. 46 (2007) 5404.
[23] T. Miyakawa, D.L. Dexter, Phys. Rev. B 1 (1970) 2961.
[24] F. Liu, E. Ma, D. Chen, Y.L. Yu, Y.S. Wang, J. Phys. Chem. B 110 (2006) 20843.
[25] J. Silver, M.I. Martinez-Rubio, T.G. Ireland, G.R. Fern, R. Withnall, J. Phys. Chem. B 105 (2001) 948.
[26] H.Q. Liu, C.F. Wu, G.S. Qin, H.Y. Lin, W.P. Qin, J. Zhan, D. Zhao, X.G. Ren, S.Z. Lu, Chin. J. Lumin. 23 (2002) 627.
[27] C.Y. Chen, R.R. Petrin, D.C. Yeh, W.A. Sibley, J.L. Adam, Opt. Lett. 14 (1989) 432.
[28] Y. Matsumoto, U. Unal, Y. Kimura, S. Ohashi, K. Izawa, J. Phys. Chem. B 109 (2005) 12748.
[29] S. Ida, U. Unal, K. Izawa, O. Altuntasoglu, C. Ogata, T. Inoue, K. Shimogawa, Y. Matsumoto, J. Phys. Chem. B 110 (2006) 23881.